Review of Scientific Instruments

EXPANSE: A time-of-flight EXPanded Angle Neutron Spin Echo spectrometer at the Second Target Station of the Spallation Neutron Source

Cite as: Rev. Sci. Instrum. **93**, 075107 (2022); https://doi.org/10.1063/5.0089349
Submitted: 24 February 2022 • Accepted: 15 June 2022 • Published Online: 11 July 2022

Changwoo Do, Rana Ashkar, Cristina Boone, et al.

Review of Scientific Instruments ARTICLE scitation.org/journal/rsi

EXPANSE: A time-of-flight EXPanded Angle Neutron Spin Echo spectrometer at the Second Target Station of the Spallation Neutron Source

Cite as: Rev. Sci. Instrum. 93, 075107 (2022); doi: 10.1063/5.0089349
Submitted: 24 February 2022 • Accepted: 15 June 2022 •
Published Online: 11 July 2022

Changwoo Do,[1,a] Rana Ashkar,[2] Cristina Boone,[3] Wei-Ren Chen,[1] Georg Ehlers,[4] Peter Falus[5] Antonio Faraone,[6] Jason S. Gardner,[7] Van Graves,[3] Thomas Huegle,[4] Reika Katsumata,[8] Darian Kent,[3] Jiao Y. Y. Lin,[3] Bill McHargue,[4] Bradley Olsen,[9] Yangyang Wang,[10] Danielle Wilson,[3] and Y Z[11,12,13]

AFFILIATIONS

[1]Neutron Scattering Division, Oak Ridge National Laboratory, Oak Ridge, Tennessee 37831, USA
[2]Department of Physics and Center for Soft Matter and Biological Physics, Virginia Tech, Blacksburg, Virginia 24061, USA
[3]Second Target Station, Oak Ridge National Laboratory, Oak Ridge, Tennessee 37831, USA
[4]Neutron Technologies Division, Oak Ridge National Laboratory, Oak Ridge, Tennessee 37831, USA
[5]Institute Laue Langevin (ILL), 71 Avenue des Martyrs, 38000 Grenoble, France
[6]Center for Neutron Research, National Institute of Standards and Technology, Gaithersburg, Maryland 20899-6102, USA
[7]Material Science and Technology Division, Oak Ridge National Laboratory, Oak Ridge, Tennessee 37831, USA
[8]Polymer Science and Engineering, University of Massachusetts Amherst, Amherst, Massachusetts 01003, USA
[9]Department of Chemical Engineering, Massachusetts Institute of Technology, Cambridge, Massachusetts 02139, USA
[10]Center for Nanophase Materials Sciences, Oak Ridge National Laboratory, Oak Ridge, Tennessee 37831, USA
[11]Department of Nuclear, Plasma, and Radiological Engineering, University of Illinois at Urbana-Champaign, Urbana, Illinois 61801, USA
[12]Beckman Institute for Advanced Science and Technology, University of Illinois at Urbana-Champaign, Urbana, Illinois 61801, USA
[13]Department of Electrical and Computer Engineering, University of Illinois at Urbana-Champaign, Urbana, Illinois 61801, USA

Note: Paper published as part of the Special Topic on New Science Opportunities at the Spallation Neutron Source Second Target Station.
[a]**Author to whom correspondence should be addressed:** doc1@ornl.gov

ABSTRACT

EXPANSE, an EXPanded Angle Neutron Spin Echo instrument, has been proposed and selected as one of the first suite of instruments to be built at the Second Target Station of the Spallation Neutron Source at the Oak Ridge National Laboratory. This instrument is designed to address scientific problems that involve high-energy resolution (neV–μeV) of dynamic processes in a wide range of materials. The wide-angle detector banks of EXPANSE provide coverage of nearly two orders of magnitude in scattering wavenumbers, and the wide wavelength band affords approximately four orders of magnitude in Fourier times. This instrument will offer unique capabilities that are not available in the currently existing neutron scattering instruments in the United States. Specifically, EXPANSE will enable direct measurements of slow dynamics in the time domain over wide Q-ranges simultaneously and will also enable time-resolved spectroscopic studies. The instrument is expected to contribute to a diverse range of science areas, including soft matter, polymers, biological materials, liquids and glasses, energy materials, unconventional magnets, and quantum materials.

I. INTRODUCTION

Neutron spin echo (NSE) is the highest energy resolution method among neutron spectroscopy techniques and the only one that directly measures correlation functions in the time domain. In fact, it has a very distinct position in neutron scattering methods by providing simultaneous access to unique time and length scales. Because of its characteristics, NSE is an essential technique for understanding atomic-scale dynamics in various systems, including hard, soft, and biological materials, and it plays an indispensable role in modern society.[1–5] However, the data acquisition rate of current NSE is generally slower than that of other neutron spectrometers, as a consequence of the relatively small detector coverage and the fact that one measures *polarization*. The NSE user community is diverse, including scientists interested in soft condensed matter, polymers and biophysics, chemical physics, as well as magnetism. The strong interest in a new NSE spectrometer from the community is evident from various workshops and reports in the past decade.[6–9] The scientific community has noted the needs for a new NSE instrument that can enable faster data collection, a wide measurement range in both length and time scales, and the use of the smaller volume of samples.

EXPANSE will incorporate wide-angle detector banks to provide approximately two orders of magnitude in the exchanged wavevector, Q-range, and a wavelength band that can provide about four orders of magnitude in Fourier times. The instrument naturally expands, with a good overlap, the dynamic ranges offered by BASIS[10] and NSE[11] at the Spallation Neutron Source (SNS) and CHESS[12] at the Second Target Station (STS) in a wide Q range, toward lower energies (slower dynamics). This instrument will provide a unique capability that is not presently available. First, EXPANSE will utilize the wide wavelength bandwidth, $\Delta\lambda \approx 4$ Å, available from STS combined with wide-angle detector modules to enable data collection over a wide momentum transfer range from 0.05 to 3.14 Å^{-1} and Fourier time range from ~30 ps to ~90 ns in a typical operation mode (NSE mode). The wide momentum transfer range (2 orders of magnitude) and Fourier time range (~4 orders of magnitude when two wavelength settings are combined) will enable pair distribution function (PDF) type data analysis by obtaining real space–time correlation function, $G(r, t)$, from Fourier transforming the intermediate scattering function, $I(Q, t)$.[13] The length and time scales covered by EXPANSE are complementary to other quasi-elastic neutron scattering (QENS) techniques. Second, the significantly enhanced source brightness [a factor of ~20 compared to the First Target Station (FTS)] will enable the possibility of time-resolved spectroscopic experiments or non-equilibrium dynamic studies. The high flux of STS will also enable EXPANSE to measure incoherent dynamics, which is currently challenging because of the inherently low signal-to-noise ratio in incoherent scattering measurements. Moreover, EXPANSE, with its high detector coverage, will be able to measure efficiently the incoherent scattering signal, which is spread over the whole scattering solid angle.

The high estimated count rate will also make studies of small samples a possibility, which will be a critical improvement for many scientific communities, especially biology and magnetism, where the sample quantity is often a severe limiting factor. A highly optimized beam for such a small volume of samples and the expanded scattering angle coverage are ideal to perform grazing incidence NSE experiments,[14,15] which is also expected to broaden the user community significantly. In addition, EXPANSE will be a hybrid in the sense that it will be equipped with a fast chopper near the sample to function as a direct geometry chopper spectrometer (DGS mode) with polarized neutrons. In this mode, the magnetic field will be turned off and time-of-flight analysis will be used to expand the energy window offered by the NSE mode (standard operation mode) by two orders of magnitude on the high energy transfer side in the range of μeV–meV while providing approximately one order of magnitude overlapping time range. This is essential for making EXPANSE a true wide-energy-range spectrometer, giving it a dynamic range of ~6 orders of magnitude if two wavelength settings are used. Finally, because of the physical principle NSE is built upon, polarization analysis naturally comes with EXPANSE. This polarization analysis, together with its wide momentum transfer coverage and a direct geometry chopper spectrometer mode, will enable the discrimination of coherent and incoherent scattering at each Q and

TABLE I. Instrument design characteristics of the EXPANSE instrument.

Property name	Characteristics
Available wavelength	4–16 Å
Wavelength band	~4 Å (15 Hz)
Incident beam divergence	<1.5°
Maximum field integral	~0.27 T m
Detector solid angle	140° × 2.5° array of ^{3}He tube detectors
Momentum transfer range	0.05–3.14 Å^{-1}
Fourier time range	30 ps–90 ns (using 4–12 Å)
Direct geometry mode	Energy resolution 10–300 μeV Incident energy range 0.5–9 meV Corresponds to 0.1–100 ps

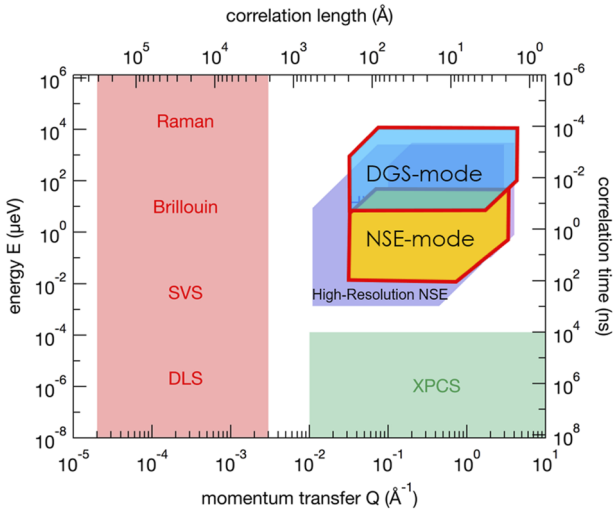

FIG. 1. Accessible energy and momentum space by EXPANSE for different modes of operation (NSE-mode and DGS-mode).

the separation of magnetic from nuclear scattering. The latter is beneficial, and sometimes essential, to the study of both soft and hard materials. The key instrument parameters of EXPANSE are summarized in Table I, and the accessible energy and momentum space are described in Fig. 1.

II. INSTRUMENT DESCRIPTION

We have calculated that the EXPANSE instrument will perform best with the tube moderator[16–18] that provides a higher time averaged flux for cold neutrons. As a result, beamport ST22 that faces the tube moderator will be an ideal location for the proposed instrument. The key instrument components are described in Fig. 2 along with their location information in Table II. Here, *F*, *M*, *R*, and *P* for the choppers stand for *frame-overlap*, *monochromatic*, *removal*, and *pulse shaping*, respectively.

A. Chopper system

EXPANSE requires a hybrid chopper system to accommodate a diffraction-style sawtooth beam at the sample for the NSE mode as well as a short-pulsed monochromatic beam with Repetition Rate Multiplication (RRM) for the DGS mode. The switch between the two modes can be a push-button operation that takes several minutes at most. In order to switch from the DGS mode to the NSE mode, the M chopper will be translated out of the beam whereas the R chopper will simply be parked in the "open" position. The chopper system is straightforward to realize and does not present technical challenges or risks.

1. NSE mode

A time–distance diagram of this mode is shown in Fig. 3(a) with two pulses with a separation of 66.667 ms (STS will operate at 15 Hz). Two frame overlap choppers at 7 m (*F* chopper) and 29 m (*P* chopper) shape the neutron wavelength band that is used. Because the *F* chopper is very close to the source, a third wavelength-defining chopper will not be needed in this mode. The location of the *P* chopper is constrained by the *M* chopper that is used in the DGS mode. EXPANSE will have a T_0 chopper, which is not shown in Fig. 3 for visual clarity since it does not influence the determination of the wavelength band. The T_0 chopper will be in the bunker (at about 12 m from the source). This chopper will block the very short prompt pulse to reduce the background but transmit all short-wavelength neutrons ($\lambda > 0.5$ Å) that may be used for the EXPANSE. Figure 3(a) shows an example of a wavelength band (4.6 Å $< \lambda <$ 8.7 Å) available in this mode without being disturbed by the prompt pulse even without the T_0 chopper. The prompt pulse is shown with a length of 5 ms, which is a conservative estimate. The leakage of neutrons with 40 Å or longer wavelength is observed but considered tolerable [Fig. 3(b)]. Their effect on the practical measurements as a

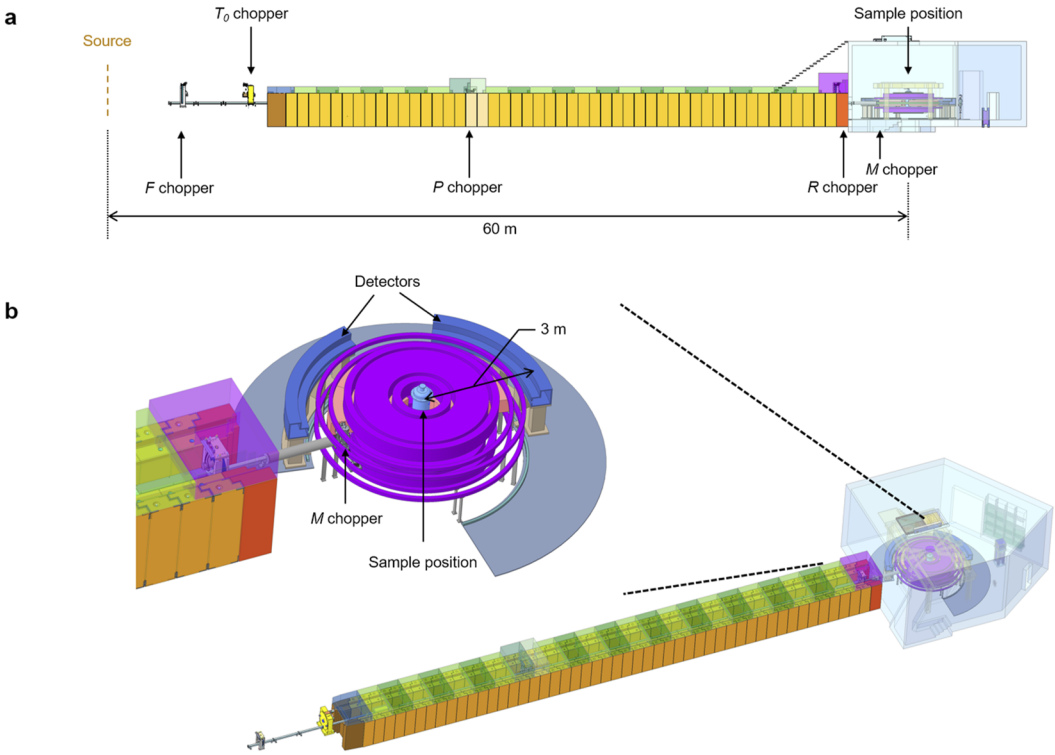

FIG. 2. Layout of instrument components of the EXPANSE. (a) Side view. (b) Perspective view. The sample area is enlarged. The source to sample distance is proposed to be 60 m. The NSE mode will utilize the frame overlap chopper (F chopper) and the pulse shaping chopper (P chopper). The DGS mode will use a short-pulsed monochromatic beam with the Repetition Rate Multiplication method, which requires an R chopper and M chopper (Fermi chopper).

TABLE II. Primary instrument components and their locations. Z is the distance from the source.

Component	Description Beam delivery	Location from moderator
Beam guide	Straight guide, m = 3	Z = 1–56 m
F chopper	1 disk @ 15 Hz	Z = 7 m (in bunker)
T_0 chopper	1 rotor @ 15 Hz	Z = 12 m (in bunker)
Operations shutter	Primary shutter for daily operations	Z = 16 m
P chopper	2 disks @ 45 Hz	Z = 29 m
Supermirror polarizer		Z = 53.5 m
R chopper	1 disk @ 90 Hz	Z = 54.7 m
Fermi chopper (*M*)	240 Hz	Z = 58 m
Beam line shielding	Bunker to cave	Z = 13.2–55.6 m
Sample location		Z = 60 m
Beam stop		Z = 66 m
Component	Description End station	Location from sample
Shield cave		Z = −4.8 to +8.3 m
Spin flippers		Various, R = 2.3 m
Detector modules	Two 70° banks of ^{3}He tubes with wide-angle polarizing analyzers	R = 2.733 m
Coils	Sample field coils	Various, R = 0.5–2.4 m

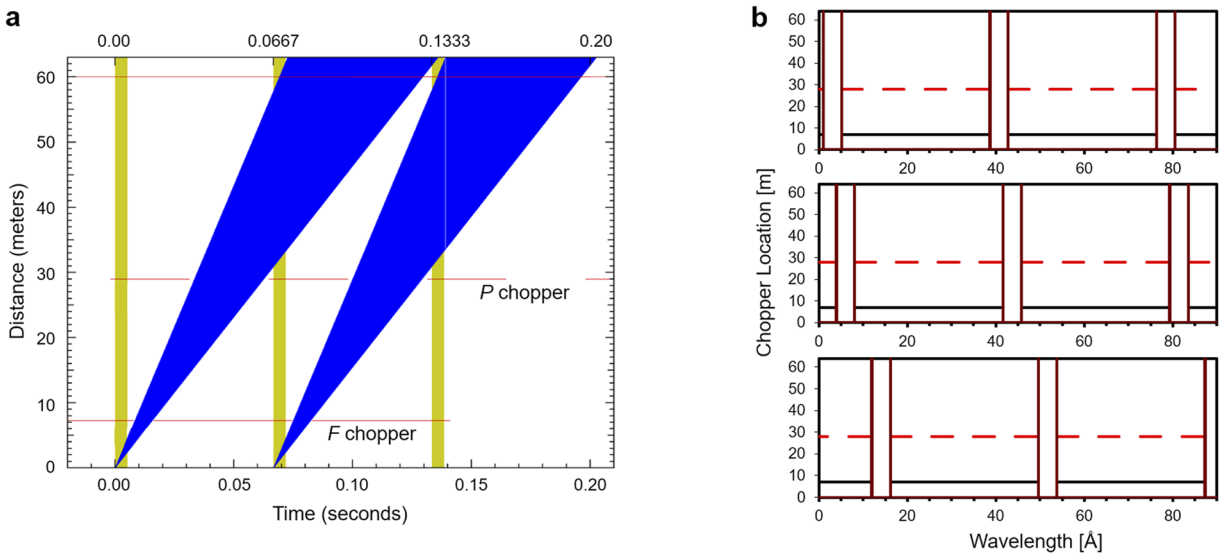

FIG. 3. (a) Time–distance diagram of EXPANSE in the NSE mode. The prompt pulse is shown with a length of 5 ms, which is a conservative estimate (yellow). (b) Leakage test for selected wavelength bands: (top) 1–5.2 Å, (middle) 4–8.2 Å, and (bottom) 12–16.2 Å.

background can be neglected since the flux of these long wavelength neutrons is several orders of magnitude lower.

2. DGS mode

A time–distance diagram of the DGS mode is shown in Fig. 4. In this mode, two more choppers are active: the *R* chopper at 54.7 m and the *M* chopper at 58 m. As the name of the mode suggests, the instrument runs as a direct-geometry inelastic spectrometer with Repetition Rate Multiplication (RRM).

In order for RRM to work, the *M* and *P* choppers need to be at commensurate distances from the source, and a ratio of 2:1 (58 m:29 m) has been chosen. The *M* chopper should be as close as rea-

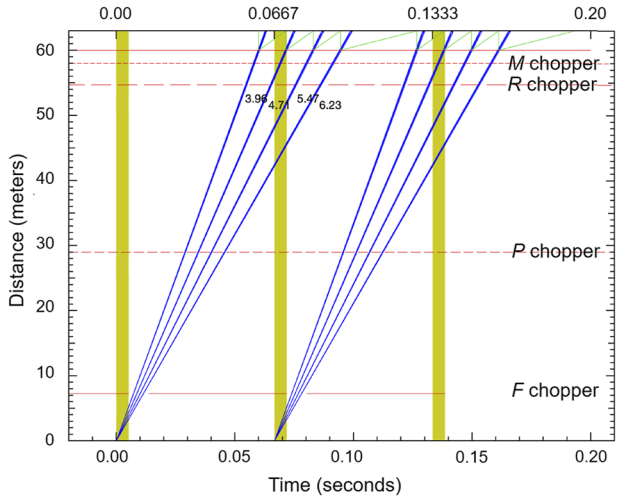

FIG. 4. Time–distance diagram of EXPANSE in the DGS mode. The prompt pulse is shown with a length of 5 ms (yellow). Four pulses are demonstrated for wavelengths 3.96, 4.71, 5.47, and 6.23 Å.

sonably achievable to the sample, and a distance of 2 m has been assumed considering the available spaces constrained by the coils. This is because the short burst time of the *M* chopper, ~50 μs for 2%–3% energy resolution with cold neutrons, needs to be effective at the sample position and not smeared out. Because of the beam size at the *M* chopper position, ~5 cm across, this chopper must be a Fermi chopper. Disk choppers will not be able to reach such burst times with this beam size. With an aspect ratio of the slit package (slit separation over length along the beam) in the range of 1:10–1:20, this chopper will have to run at 180–240 Hz to achieve the desired burst time. We evaluated that it is not necessary to push for higher energy resolution in the DGS mode because the NSE mode will provide a good resolution. It is desirable to have a reasonable overlap between the two modes in terms of the energy resolution they offer. Since the *M* chopper is not needed in the NSE mode, and as a Fermi chopper, it cannot be parked open, this chopper will be removed from the beam via horizontal or vertical translation. Technical solutions for such a motion exist at ARCS, SEQUOIA, or CNCS at the FTS.

The *R* chopper will be a pulse removal chopper and will select one out of 4–6 pulses that the *M* chopper allows. This pulse suppression factor will depend on the wavelength chosen and on how much energy loss one will want to cover in time of flight. In this regard, Fig. 4 assumes a rather short lead wavelength of 4 Å and that, for each pulse, 90% energy loss is desired. In this situation, the *R* chopper will need to open six times per source pulse, making it a 90 Hz chopper with a single slit. Two of the six pulses, as shown in Fig. 4, are removed by the *F* chopper in the front. The *R* chopper does not have to provide sharp pulse edges, as it will only remove pulses. For this reason, it can be a slow (90 Hz) disk chopper. However, it cannot be arbitrarily far away from the *M* chopper because it still needs to run synchronously. This effect is illustrated in Fig. 4 as the *R* chopper opening is well centered for the 3.96 Å pulse but not for the 6.23 Å pulse. It is estimated that the distance between the *M* and *R* choppers can be increased to 4 m without a loss of functionality.

The *P* chopper will be at half the distance from the source as the *M* chopper. In the DGS mode, the *P* chopper will open twice as often as the *R* chopper. Figure 4 illustrates a situation where the *P* chopper opens 12 times per source pulse, which is probably the highest opening frequency ever needed. The *P* chopper can be a disk chopper because, much like the *R* chopper, it removes pulses but does not have to provide sharp pulse edges. In the NSE mode, this chopper opens only once per pulse for half the time. Figure 5 shows how this double functionality (DGS mode and NSE mode) can be technically achieved. The *P* chopper can be a double disk chopper with two identical disks that run in the same rotational sense (for example, clockwise). By re-phasing the disks relative to each other, one can achieve openings of equal length either four times per revolution or two times per revolution. Together with the additional degree of freedom of the chopper speed, all desired modes of operation can be configured. The *F* chopper at ~7 m is a single-disk working at 15 Hz. The single opening of the disk should be around 40° wide.

3. Energy resolution in DGS mode

The energy resolution of the instrument is given by three terms as follows:[12,19,20]

$$\delta\hbar\omega = m_n \cdot \left[v_1^2 \cdot \delta v_1^2 + v_2^2 \cdot \delta v_2^2 + v_3^2 \cdot \delta v_3^2\right]^{\frac{1}{2}}, \quad (1)$$

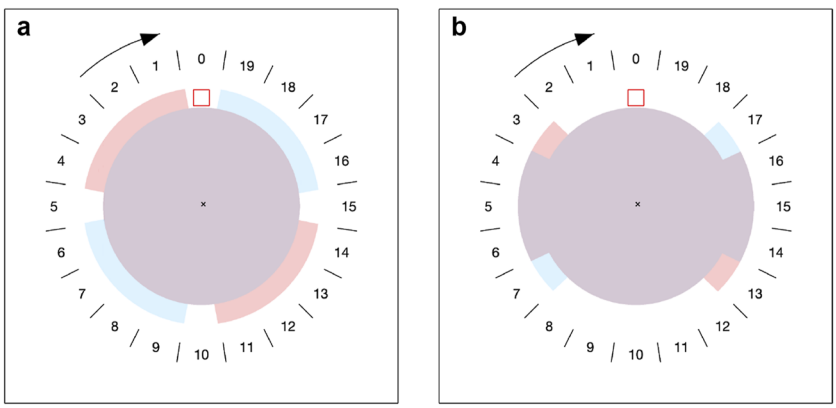

FIG. 5. *P* chopper in the DGS mode at 45 Hz (a) and in the NSE mode at 7.5 Hz (b). The red square is the beam. The numbered sectors are for reference only.

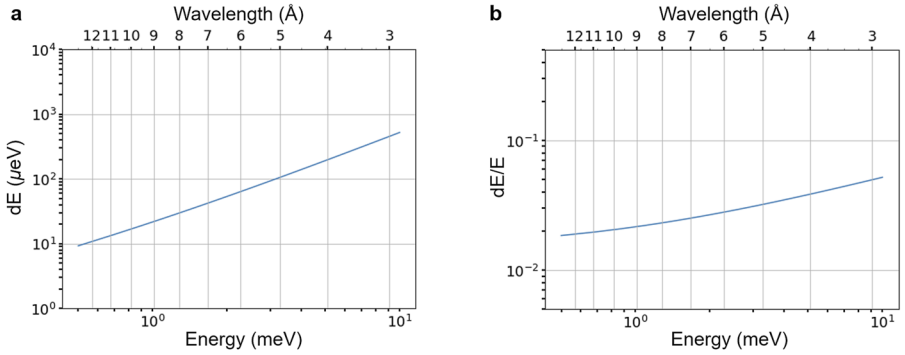

FIG. 6. Estimated energy resolution of the elastic scattering line. (a) dE and (b) dE/E.

where

$$v_1^2 \cdot \delta v_1^2 = \left(\frac{v_i^3}{L_1} + \frac{v_f^3 L_2}{L_1 L_3} \right)^2 \cdot \delta t_1^2, \tag{2}$$

$$v_2^2 \cdot \delta v_2^2 = \left(\frac{v_i^3}{L_1} + \frac{v_f^3 (L_1 + L_2)}{L_1 L_3} \right)^2 \cdot \delta t_2^2, \tag{3}$$

$$v_3^2 \cdot \delta v_3^2 = \left(\frac{v_f^3}{L_3} \right)^2 \cdot \delta t_3^2. \tag{4}$$

Here, $v_{i,f}$ are the incident and final velocities, respectively, and m_n is the mass of a neutron. The distance and timing uncertainties can be interpreted in two ways, depending on where the pulse is initially defined: in the source or in the first of two high-speed choppers. In the first case, L_1 is the distance between the source and the M chopper, and δt_1 is the pulse length at the source. In the second case, the P chopper is considered the source, L_1 is the distance between the two choppers (P to M), and δt_1 is the opening time of the first (P) chopper. Furthermore, L_2 is the distance from the second (M) chopper to the sample, L_3 is the distance from the sample to the detector, δt_2 is the opening time of the second chopper, and δt_3 is the uncertainty in time-of-flight between the sample and the detector. The last term can be further broken down, into contributions from the timing resolution of the detector, and the effects of sample size and pixel size. The instrument design will aim for these three terms to be roughly of the same size, as this will result in optimal resolution vs intensity in the detector. In Fig. 6, energy resolution for the elastic scattering line is estimated based on the following three assumptions. (1) A pulse width of STS can be expressed as $v\delta t_1 \approx 0.23$ m on average,[12,20] (2) a Fermi chopper slit package capable of $\delta t_2 = 50$ μs, and (3) 1 cm distance uncertainty for $\delta t_3 = 1(\text{cm})/\text{V}$. The estimation shows that the DGS mode will provide energy resolution of 10–300 μeV that corresponds to dE/E = 1.8%–5%.

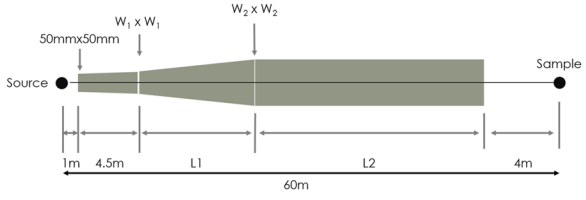

FIG. 7. Guide configuration considered for the simulation.

B. Beam transport system

In order to understand the beam characteristics of the instrument, simulations were performed using McStas version 2.6.1.[21,22] Dimensions of the neutron guides are optimized using a few constraints as described in Fig. 7. First, the source-to-sample distance was fixed to be 60 m considering the potential location of the instrument. Second, a square guide cross section was assumed as a first approximation. Third, the initial opening dimension facing the source was fixed to be 50 × 50 mm^2 following the description of monolith optics described in the technical document of the STS.[23–25] The monolith guide ends at about 5.5 m from the source. The cross section of the guide within the monolith expands slightly to W_1. A tapered guide continues for a length D_1 whose exit dimension is W_2. The rest of the guide was assumed to be straight with a square cross section. These dimensions (W_1, W_2, D_1, and D_2) were obtained to provide the best flux at the sample that is assumed to be 1 × 1 cm^2. Notably, this sample size that the EXPANSE instrument is aiming to achieve is much smaller than the conventional NSE sample size (3 × 3 cm^2). The large sample volume, which is often required for conventional NSE, has been a long-standing barrier for some areas of science to use NSE techniques. Therefore, the EXPANSE will open new opportunities for research areas where sample volumes are limited.

The optimized guide with W_1 = 65 mm, W_2 = 90 mm, D_1 = 19 m, and D_2 = 31.5 m provided ~314% increase in total flux (4–16 Å) and 353% in the long wavelength flux (12–16 Å) compared to the flux expected from the fully straight guide with 50 × 50 mm^2 cross section. For this geometrical optimization, all guide m-values are assumed to be 8. Here, m-value refers to the multiplicative increase in the critical angle over that of the Ni-coated neutron guide. However, after the geometrical optimization, the m-value was varied and the flux was predicted to be practically the same for all m-values greater than 3. The time-averaged flux expected at the sample is shown in Fig. 8(a). Blue markers indicate the theoretical flux at the sample using the guide configuration described above. For a comparison, flux profiles from the First Target Station neutron spin echo instrument (FTS-NSE) are shown together.[11] According

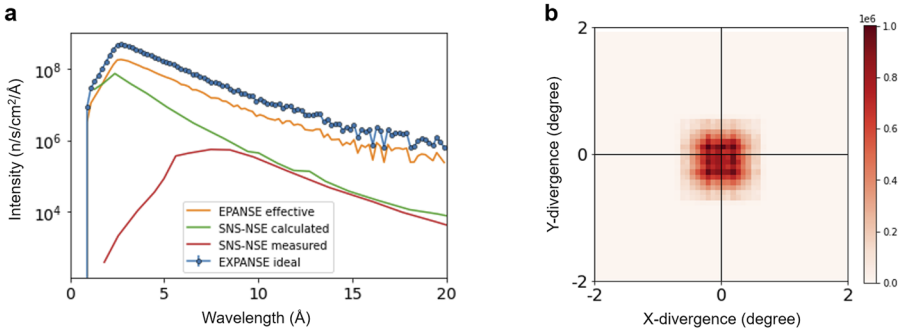

FIG. 8. (a) Comparison of the flux at the sample position: as simulated (blue markers) from the McStas simulation and after multiplying several attenuation factors (orange). Fluxes from SNS-NSE[11] are shown for comparison (green and red solid lines). (b) Divergence of the neutrons arriving at the sample position (1×1 cm^2).

to the reference, the SNS-NSE calculated flux was multiplied by several attenuation factors, such as 0.5 to account for polarization, 0.85 to account for geometrical shadowing in the bender, 0.9 for bender reflectivity, and 0.98 to account for chopper gaps in the neutron guide. While the geometrical shadowing factor and the bender reflectivity may not be applicable to the EXPANSE, the same factors have been multiplied to the ideal flux (blue markers) to obtain the effective flux, in a conservative way, for the EXPANSE (orange solid line). Overall, the proposed guide configuration provides ~2–10 times neutron flux of the SNS-NSE depending on the wavelength, which properly reflects the increased time-averaged flux of the STS source (700 kW, 15 Hz) compared to that of the FTS (1.4 MW, 60 Hz). The divergence profiles of neutrons arriving at the sample position (1×1 cm^2 area) satisfy the small divergence condition (<1°), required for a neutron spin-echo instrument [Fig. 8(b)].

C. Coils and magnetic field

The design of the wide-angle spin echo instrument requires four sets of coils shown in Fig. 9, main precession coils, compensation coils 1 (cc1), compensation coils 2 (cc2), and sample field coils. These coils are not connected to the moving parts of the spectrometer and are designed to provide stable and steady magnetic fields for NSE operation. Each coil pair is mounted in a co-axial fashion, situated symmetrically relative to the horizontal scattering plane. The direction of the current for each coil pair is described in Fig. 9(b) with plus and minus signs. This setup ensures the symmetry in the magnetic field so that it does not change with the scattering angle. Therefore, the condition for simultaneous NSE measurements over a wide angular range is satisfied.

The main precession coils have anti-parallel electric currents. As a result, the magnetic field along the scattering plane is horizontal and becomes zero at the sample position. The shape and size of the main precession coils and the field generated by them determine the maximum field integral for the NSE operation. Here, we aim to have maximum field integral of 0.25 T•m, which corresponds to the longest Fourier time [$\tau(ns) = 0.186\,358\phi\lambda^3$, ϕ is the field integral (T m) and λ is the wavelength (Å)] of 80 ns with 12 Å and 3 ns with 4 Å wavelength neutrons. The sample field coils have small parallel electric currents and produce a weak and homogeneous vertical field at the sample position, which maintains the axial symmetry required in the magnetic configuration. The pairs of compensation coils (cc1, near the precession coils) have anti-parallel electric currents and provide a counter field against the main precession field. The major role of these coils is to reduce the radial field around the sample and π-flipper, and around the outer π/2-flipper coils. The outer compensation coils (cc2) fine tune the radial magnetic field at the position of the π/2-flipper. While Fresnel coils are omitted for visual clarity in Fig. 9, they will be required to correct field inhomogeneities away from the central beam axis. Two rings of Fresnel coils will be used to provide a quadratic correction field located near the inner and outer diameter of the precession coil.

Using the coil geometry given in Fig. 9(b), the magnetic field profile has been calculated using the Biot–Savart law. With 810 000 A turn current, a field integral of 0.256 T m is estimated starting from the position of the $\pi/2$-flipper position until the

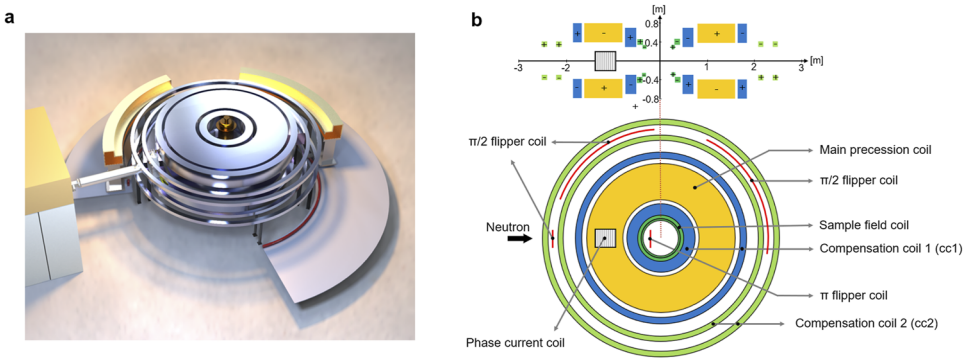

FIG. 9. Details of the coil arrangement for the EXPANSE. (a) 3D engineering model. (b) Schematics of side and top views of the key components of the EXPANSE.

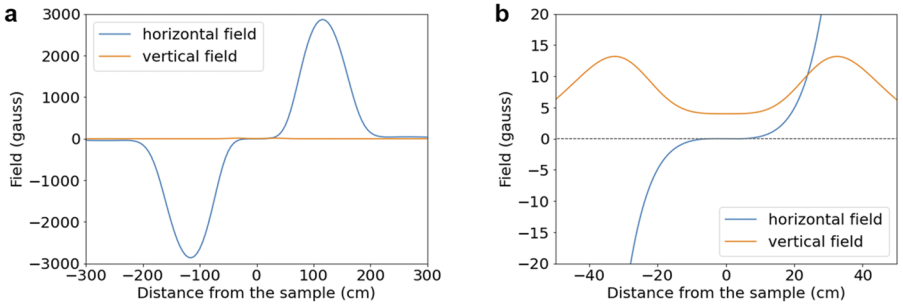

FIG. 10. (a) Magnetic field profiles across the instrument dimension. (b) Magnetic field profiles around the sample area. Fields were calculated using the 810,000 A turn current of the main precession coil producing a field integral of 0.256 T m. The dotted line is the zero-field axis.

π-flipper. This corresponds to an 800 A current with wires that have a 2×2 cm^2 cross section. For comparison, a similar instrument built at ILL (WASP) used wires with a 2.5×2.5 cm^2 cross section with 800 A at a tension of 500 V, which is produced by commercially available standard magnet power supplies. Figure 10(a) shows the overall field for this field integral setting. The field profile around the sample is shown in Fig. 10(b). The π-flipper can be placed at around 10 cm from the sample where the field is vertical and weak enough. Assuming that the lowest field integral that can be practically used is 0.0025 T m, the accessible Fourier time range is expected to be 29 ps $< \tau <$ 3 ns with 4 Å neutrons, 239 ps $< \tau <$ 24 ns with 8 Å neutrons, and 800 ps $< \tau <$ 82 ns with 12 Å neutrons.

One of the biggest potential sources of depolarization in a wide-angle NSE spectrometer is the turning of the magnetic field direction from a horizontal to a vertical direction in the sample area of the instrument. Polarization can be lost when the direction of the magnetic field changes quicker than the Larmor frequency of the neutron spins.[26,27] A typical guiding figure for determining the likelihood of depolarization due to such nonadiabatic field changes is the adiabaticity parameter A,

$$A = \frac{\omega_B}{\omega_L} = \frac{\omega_B}{\gamma B},$$

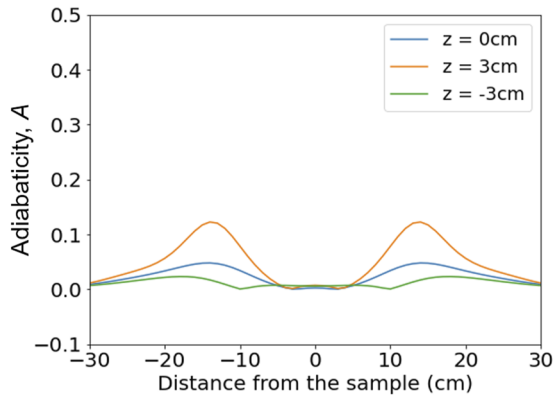

FIG. 11. Adiabaticity calculated with the maximum field integral condition assuming neutron wavelength of 4 Å. Different heights of the neutron path deviating from the center of the scattering plane have been considered.

TABLE III. Accessible Fourier time ranges for representative selections of the wavelength band and the field integral.

Wavelength band (Å)	Field integral (T m)	Fourier time range
4–8	0.0025	29 ps $< \tau <$ 238 ps
	0.256	3 ns $< \tau <$ 24 ns
8–12	0.0025	238 ps $< \tau <$ 805 ps
	0.256	24 ns $< \tau <$ 82 ns
12–16	0.0025	0.8 ns $< \tau <$ 1.9 ns
	0.256	82 ns $< \tau <$ 195 ns

where ω_B is the rate of change of the direction of the B field and ω_L is the Larmor frequency of the neutron spin. It is suggested that the polarization losses will be small if A is below 0.2. In Fig. 11, the adiabaticity parameter has been calculated with 4 Å wavelength, which is likely the fastest neutron wavelength used for the spin-echo operation. If the adiabaticity condition is satisfied with a short wavelength neutron, the same is guaranteed for the slower neutrons. To consider the finite sizes of the beam and the sample, different distances of the neutron path to the beam axis have been considered. As the calculation indicates, the maximum adiabaticity value does not exceed 0.15 even for the neutrons traveling ±3 cm away vertically from the scattering plane. In Table III, the accessible Fourier times with selected wavelength bands are summarized. The unique advantage of the EXPANSE over the existing wide-angle neutron spin echo instrument (WASP) is that ranges of Fourier times can be accessed simultaneously by using neutrons with different energies. Since the Fourier time is proportional to λ^3, the widest dynamic range in the time-domain can be obtained from the short wavelength band, 4–8 Å. With this wavelength band, approximately an order of magnitude of dynamic ratio ($\frac{\tau_{long}}{\tau_{short}} = \frac{8^3}{4^3} = 8$) can be expected at given field integral setting. This suggests that potential kinetic studies can be done, for the first time with neutron spin echo, if a small window of Fourier time range is suitable.

***π*-flipper**. Using the gyromagnetic ratio of the neutron (2916 Hz/G), the field strength required for π precession turn can be estimated. For example, 17 G cm flipper field integral is needed to achieve a complete π-flip for 4 Å neutrons. The π-flipper will be located near the sample where the horizontal field is minimal. The vertical guide field will be compensated inside the flipper to be zero. The flipper field will be tuned according to the wavelength. Figure 12(a) shows the required field to perform a perfect π-flip

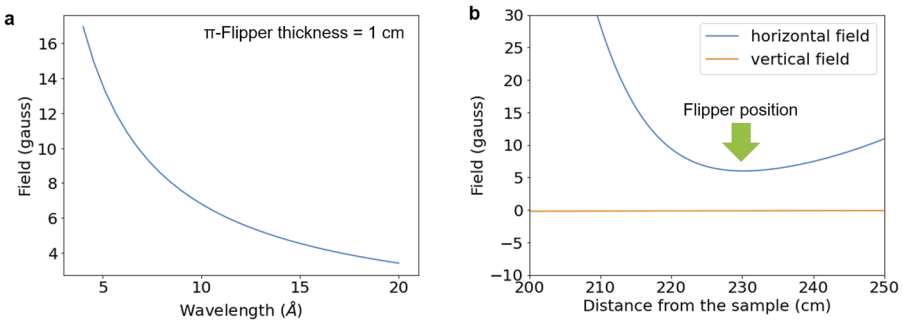

FIG. 12. (a) Flipper field required for a complete π-turn as a function of wavelength. (b) Guide fields around the $\pi/2$-flipper position that have been tuned for $\pi/2$ spin–flip of 8 Å neutrons with a 1 cm flipper coil thickness.

using a flipper of 1 cm thickness. In practice, the current of the flipper coil will have a time-dependent profile to satisfy the flipper field requirement. The time-dependent current profile will be synchronized with the source pulse so that the appropriate flipper field is prepared for neutrons with different wavelengths.

***π*/2-flipper**. In the $\pi/2$-flip, the spin essentially precesses one-half turn around an inclined axis (45° relative to the outer field direction). Therefore, the outer guide field (horizontal field) needs to be tuned first using the outer compensation coils (cc2) in Fig. 9. The ideal guide field for this $\pi/2$-flip should have a flat constant horizontal field component B_x over the thickness of the flipper (~1 cm), and $\sqrt{2}B_x$ should satisfy the one-half turn precession condition. For example, for the 8 Å neutrons, 8.48 G flipper field is needed for the one-half turn during 1 cm travel. Therefore, $\sqrt{2}B_x = 8.48, B_x = 6$ gauss, horizontal guide field is required. Figure 12(b) shows that the horizontal guide field (B_x) can be tuned using the compensation coils (cc2) to match the required field strength at the $\pi/2$-flipper position (x = 230 cm). In practice, incident neutrons will go through a dedicated $\pi/2$-flipper and the scattered neutrons will go through arc shaped $\pi/2$-flippers covering a 70° scattering angle each. The arc shape $\pi/2$-flippers will be part of the 70 analyzer/detector bank so that they will move together if needed [Fig. 9(b)].

Range of the stray field. Since a strong magnetic field will be constantly used for the operation of the EXPANSE instrument, the potential influence on the nearby instruments or equipment that are sensitive to the magnetic field has been considered. According to the calculation, the highest field integral setting will generate a horizontal field strength of 1 G at about 8 m distance from the sample (Fig. 13). At a 10 m distance from the sample, it is expected that the field strength will be reduced to the level of the earth's magnetic field (0.25–0.65 G).[28] Therefore, the interference to the nearby beamlines will be negligible if the EXPANSE spectrometer is built at the proposed ST22 location, which is already well separated from other instruments.

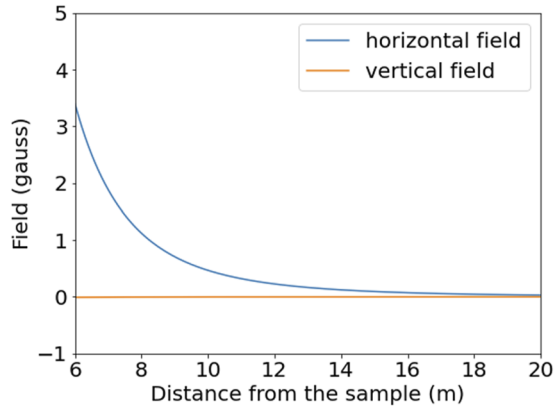

FIG. 13. Magnetic field profile over a long distance generated from the EXPANSE instrument at the maximum field integral setting.

D. Analyzers and detectors

The analyzer design will follow the demonstrated precedent that is based on Schärpf-type C-shaped benders and used at the WASP instrument (ILL, France).[27,29,30] The supermirror of selected m-values (Co/Ti with m = 2.8 is assumed at present) are double-side coated and mounted into cassettes that will hold the mirrors with a required bending radius (8 m, targeting cutoff wavelength of about 3.5 Å). Each cassette of 260 × 160 × 50 mm^3 size will hold 40 mirrors of about 254 × 145 mm^2 area and cover roughly 1° of scattering angle at about 2.7 m from the sample (Fig. 14). Approximately 65 of these cassettes will be mounted in one bank of the analyzer-detector module to cover 70° of scattering angle. Therefore, the total supermirror coating area will be roughly 380 m^2. At the end of the analyzers, position sensitive ^{3}He detector tubes of 15 cm length will be arrayed in a single-layer configuration. Each detector tube has a diameter of 25.4 mm, and the center-to-center distance will be kept at 27 mm. This allows 2 detector tubes to face one cassette, and a total of at least 260 detector tubes will be required to cover two 70° scattering angles. The analyzer modules will be placed

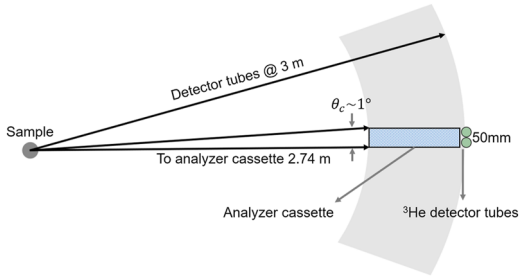

FIG. 14. Schematic showing the analyzer cassette and detector tube arrays.

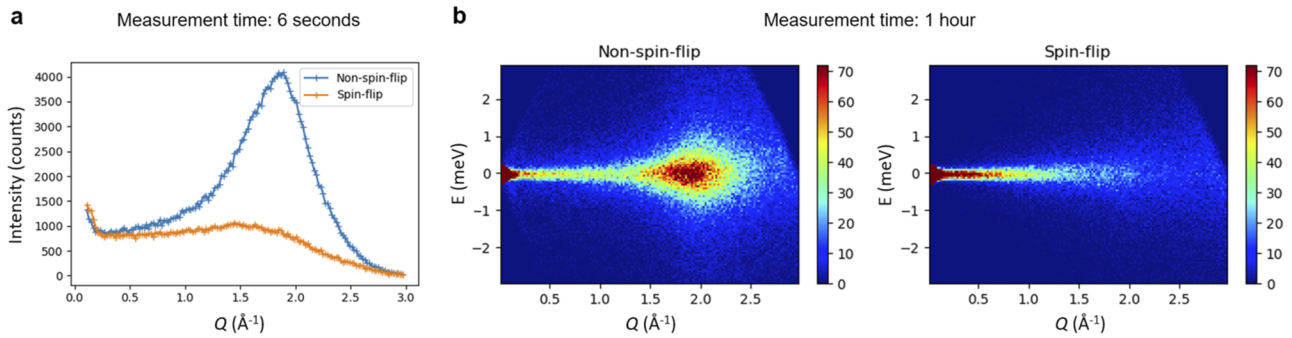

FIG. 15. MCViNE simulation results for heavy water in (a) NSE mode for 6 seconds measurement time using 4–8 Å neutron beam, and (b) DGS mode for 1 h measurement time using a 4 Å beam with a 50 μs time-of-flight width at the Fermi chopper position. The neutron beam size at the sample was 1 × 1 cm^2. A cylindrical sample geometry with a 1 cm diameter annulus with 0.5 mm thickness and 3 cm height was used.

on a vertical stage so that they can be moved out of the scattering plane for DGS mode, if needed.

E. Performance prediction

In order to estimate the performance of the proposed instrument, a virtual experiment, for a heavy water sample using both the NSE mode and the DGS mode, has been performed using the MCViNE software.[31,32] The instrument optics simulations follow the standard EXPANSE neutron optics model (Fig. 7), and a 1 × 1 cm^2 beam is focused on the sample position. In the NSE mode, the neutrons with a wavelength band of 4–8 Å are considered. In the DGS mode, a 4 Å beam was used with a 50 μs time-of-flight width at the Fermi chopper position. The neutron flux reduction caused by the polarizer is considered to be 50%, while that of the analyzer is modeled by a phenomenological model of the HYSPEC (SNS) polarization analyzer for its transmission and, in addition, by a ray-tracing component for its acceptance angle correction.[33] The sample is a 1 cm diameter annulus with 0.5 mm thickness and 3 cm height. The sample scattering kernel considers both the incoherent and coherent scattering, in which vibrational and diffusional contributions are included.[34] The detector in the simulation is in a cylindrical configuration with a radius of 3 m from the sample. The detectors are 15 cm high, and the angular spacing between them is defined by 25.4 mm/3 m ≈ 0.0085 rad. The data collected by these detectors are then reduced to $I(Q)$ for the NSE mode measurement and $I(Q, E)$ for the DGS mode measurement (Fig. 15). The elastic scattering data for the NSE mode represent a dataset collected for 6 s. The diffraction scan shown in Fig. 15(a) is often performed in the traditional high-resolution NSE instruments before echo measurements and provides a good referent to determine data collection time. Because the solid angle covered by the detectors of EXPANSE is ~20 times more than that is covered by a single configuration of high-resolution NSE, the efficiency of such a diffraction measurement is significantly improved as compared to the order of minutes. This also suggests that the echo measurements will be comparably more efficient than those from the traditional high-resolution NSE. The $I(Q, E)$ data for the DGS mode are simulated to demonstrate measurements for 1 h long data collection at the EXPANSE using a single pulse of a 4 Å beam at 15 Hz source frequency. In practice, as shown in Fig. 4, four pulses of neutron beams with different wavelengths can be used via a RRM method per a source pulse at 15 Hz. Therefore, the actual efficiency of measurements can be further increased.

F. Sample environment

Samples will be located at the center of the coils. The instrument will be designed to adapt to standard STS sample environments of a cylindrical type such as the standard orange cryostat as long as their components are non-magnetic. Therefore, the accessible temperature range will be ~1.5–1300 K covering temperature ranges desired for wide ranges of materials. The cage and the mezzanine of the EXPANSE instrument have openings that have access to the sample position. The facility crane will be available to deliver sample equipment through this opening (Fig. 16). A standard sample environment will be developed along with the instrument focusing on multiple sample loading capability. It is expected that at least five samples can be accommodated simultaneously in vertical arrays, where quartz, Nb, or Al cells with temperature variation capability that ranges from −20 to 300 °C, will be loaded from the top. A trench is designed to provide access to the sample areas from the

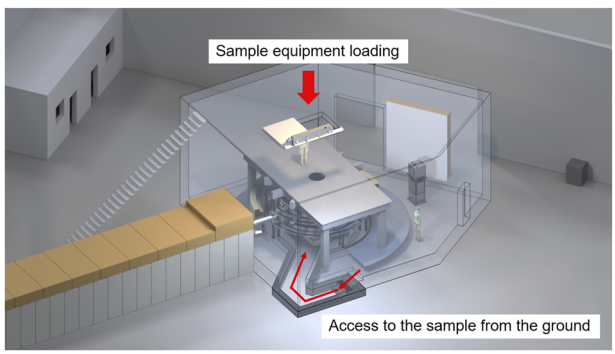

FIG. 16. Engineering model showing the opening for loading sample equipment and the access pathway to the sample from the ground level.

floor level. For the standard sample environment, users will be able to swap samples quickly by accessing the sample area through this trench.

III. SUMMARY

The first time-of-flight wide-angle neutron spin echo spectrometer on a Spallation Neutron Source in the world will be built at the ST22 beamport of the Second Target Station (STS) at the Oak Ridge National Lab. The spectrometer will combine high neutron flux, wide wavelength bandwidth, and wide scattering angle coverage that will enable fast measurements for NSE experiments over wide length and time scales, even allowing the possibility of exploring dynamics in nonequilibrium systems. The proposed instrument characteristics of ~0.25 T m field integral and a solid angle for detectors of 0.12 sr will achieve ~20 times the solid angle of the NSE at the First Target Station (FTS, BL-15). Multiplying this with 20 times increased source brightness over the FTS leads to a **gain factor of 400** over the existing NSE at the FTS, if the same amount of information is obtained over all scattering angles. Overall, EXPANSE will be a work-horse wide-angle neutron spin-echo spectrometer, and it will take a unique position in the neutron spectroscopy instrument suite in the North America.

ACKNOWLEDGMENTS

This research used the resources of the Spallation Neutron Source Second Target Station Project at the Oak Ridge National Laboratory (ORNL). ORNL is managed by UT-Battelle LLC for DOE's Office of Science. A.F. acknowledges support by the Center for High Resolution Neutron Scattering, a partnership between the National Institute of Standards and Technology and the National Science Foundation under Agreement No. DMR-2010792. The authors thank Jill Hemman (ORNL) for providing rendering images of the engineering model of the EXPANSE. The authors greatly thank all the researchers who have shown their support in the instrument proposal supporting letter (alphabetical order): Mikael Andersson, Piero Baglioni, Nitash P. Balsara, Frank Bates, Wim Bras, Craig M. Brown, Zimei Bu, Sow-Hsin Chen, Wei Chen, Shiwang Cheng, Sung-Min Choi, Mike Crawford, Theo Dingemans, Michelle Dolgos, Takeshi Egami, Bela Farago, Giovanni Ferraro, Michael R. Fitzsimmons, Emiliano Frantini, Paola Gallo, Martin Gruebele, Xiaodan Gu, Monika Hartl, Olaf Holderer, Kunlun Hong, Maths Karlsson, Elizabeth Kelley, Ken Kelton, Boris Khaykovich, Tae-Hwan Kim, Abigail Knight, Maiko Kofu, Sanat Kumar, Marco Laurati, Seung-Hun Lee, Peter K. Liaw, Emily Liu, Yun Liu, Despina Louca, Rosangela Mastrangelo, Koichi Mayumi, Magdaleno Medina-Noyola, Michael Monkenbusch, Adam J. Moule, Michihiro Nagao, Jonathan Nickels, Michael Ohl, Catherine Pappas, Fyl Pincus, Roger Pynn, Shuo Qian, Dieter Richter, Simon Rogers, Thomas Russell, Makina Saito, Mark Schlossman, Yuya Shinohara, Michael Short, Sunil Sinha, Jeff Sonier, Matthew Tirrell, Madhusudan Tahi, Terrence J. Udovic, Norman Wagner, David Weitz, Christopher Wiebe, Karen Winey, Donghui Zhang, Piotr Zolnierczuk, and Reiner Zorn.

This Notice will be removed for publication:

This manuscript has been authored by UT-Battelle LLC under Contract No. DE-AC05-00OR22725 with the US Department of Energy (DOE). The US government retains and the publisher, by accepting the article for publication, acknowledges that the US government retains a nonexclusive, paid-up, irrevocable, worldwide license to publish or reproduce the published form of this manuscript, or allow others to do so, for US government purposes. DOE will provide public access to these results of federally sponsored research in accordance with the DOE Public Access Plan (http://energy.gov/downloads/doe-public-access-plan).

AUTHOR DECLARATIONS

Conflict of Interest

The authors have no conflicts to disclose.

DATA AVAILABILITY

The data in this article are available from the corresponding author upon reasonable request.

REFERENCES

[1]National Academies of Sciences, *Frontiers of Materials Research: A Decadal Survey* (National Academies Press, 2019), a Consensus Study Report of the National Academies of Sciences, Engineering, and Medicine. Available at http://doi.org/10.17226/25244

[2]See http://nsfpolymerworkshop2016.cems.umn.edu for report of a NSF Workshop, Frontiers in Polymer Science and Engineering.

[3]U.S. Department of Energy, From Quanta to the Continuum: Opportunities for Mesoscale Science, BES Workshop Report, 2012.

[4]U.S. Department of Energy, Computational Materials Science and Chemistry: Accelerating Discovery and Innovation through Simulation-Based Engineering and Science, Basic Energy Science Workshop Reports, 2010.

[5]U.S. Department of Energy, Basic Energy Sciences Roundtable Opportunities for Basic Research for Next-Generation Quantum Systems, Basic Energy Science Workshop Reports, 2017.

[6]Grand Challenges in Soft Matter (https://Neutrons.Ornl.Gov/Sites/Default/Files/Final Report-Grand Challenges in Soft Matter_Santa Barbara-v3.Pdf), 2014.

[7]Oak Ridge National Laboratory, Workshop Report: Future and Current Use of Neutron Spin-Echo Spectroscopy in Condensed Matter Research (Internal Document), 2015.

[8]Oak Ridge National Laboratory, Workshop Report: Neutron Spin Echo for Slow Dynamics Investigation (Internal Document), 2016.

[9]R. Ashkar, H. Z. Bilheux, H. Bordallo, R. Briber, D. J. E. Callaway, X. Cheng, X.-Q. Chu, J. E. Curtis, M. Dadmun, P. Fenimore *et al.*, "Neutron scattering in the biological sciences: Progress and prospects," Acta Crystallogr., Sect. D: Struct. Biol. **74**, 1129–1168 (2018).

[10]E. Mamontov and K. W. Herwig, "A time-of-flight backscattering spectrometer at the spallation neutron source, BASIS," Rev. Sci. Instrum. **82**(8), 085109 (2011).

[11]M. Ohl, M. Monkenbusch, N. Arend, T. Kozielewski, G. Vehres, C. Tiemann, M. Butzek, H. Soltner, U. Giesen, R. Achten *et al.*, "The spin-echo spectrometer at the spallation neutron source (SNS)," Nucl. Instrum. Methods Phys. Res., Sect. A **696**, 85–99 (2012).

[12]G. Sala, J. Y. Y. Lin, V. B. Graves, and G. Ehlers, "Conceptual design of CHESS, a new direct-geometry inelastic neutron spectrometer dedicated to studying small samples," J. Appl. Crystallogr. **51**(2), 282–293 (2018).

[13]Y. Shinohara, R. Matsumoto, M. W. Thompson, C. W. Ryu, W. Dmowski, T. Iwashita, D. Ishikawa, A. Q. R. Baron, P. T. Cummings, and T. Egami, "Identifying water-anion correlated motion in aqueous solutions through van hove functions," J. Phys. Chem. Lett. **10**(22), 7119–7125 (2019).

[14]O. Holderer, H. Frielinghaus, S. Wellert, F. Lipfert, M. Monkenbusch, R. von Klitzing, and D. Richter, "Grazing incidence neutron spin echo spectroscopy: Instrumentation aspects and scientific opportunities," J. Phys.: Conf. Ser. **528**, 012025 (2014).

[15]J. Witte, P. Krause, T. Kyrey, A. M. Dahl, J. Lutzki, B. V. K. J. Schmidt, M. Ganeva, A. Koutsioubas, O. Holderer, and S. Wellert, "Grazing incidence neutron spin echo study of poly(*N*-isopropylacrylamide) brushes," Macromolecules **53**(5), 1819–1830 (2020).
[16]F. X. Gallmeier, W. Lu, B. W. Riemer, J. K. Zhao, K. W. Herwig, and J. L. Robertson, "Conceptual moderator studies for the spallation neutron source short-pulse second target station," Rev. Sci. Instrum. **87**(6), 063304 (2016).
[17]F. X. Gallmeier, T. Hügle, E. B. Iverson, W. Lu, and I. Remec, "Options for a very cold neutron source for the second target station at SNS," J. Phys.: Conf. Ser. **1021**(1), 012083 (2018).
[18]I. Remec and F. X. Gallmeier, "Neutronics analyses for the conceptual design of the SNS second target station," J. Neutron Res. **22**(2–3), 265–273 (2020).
[19]J. M. Carpenter, D. L. Price, and N. J. Swanson, IPNS - A National Facility for Condensed Matter Research, Argonne National Laboratory, 1978.
[20]G. Ehlers, A. A. Podlesnyak, J. L. Niedziela, E. B. Iverson, and P. E. Sokol, "The new cold neutron chopper spectrometer at the spallation neutron source: Design and performance," Rev. Sci. Instrum. **82**(8), 085108 (2011).
[21]P. Willendrup, E. Farhi, E. Knudsen, U. Filges, and K. Lefmann, "McStas: Past, present and future," J. Neutron Res. **17**, 35–43 (2014).
[22]P. K. Willendrup and K. Lefmann, "McStas (i): Introduction, use, and basic principles for ray-tracing simulations," J. Neutron Res **22**, 1–16 (2020).
[23]See https://neutrons.ornl.gov/sts/documents for Technical Design Report Second Target Station.
[24]See https://neutrons.ornl.gov/sites/default/files/STS_CDR_Vol1_v2.pdf for Spallation Neutron Source Second Target Station Conceptual Design Report Volume 1: Overview, Technical and Experiment Systems.
[25]See https://neutrons.ornl.gov/sites/default/files/STS_CDR_Vol2.pdf for Spallation Neutron Source Second Target Station Conceptual Design Report, Volume 2: Conventional Facilities.
[26]F. Mezei, "The principles of neutron spin echo," in *Neutron Spin Echo* (Springer, Berlin, Heidelberg, 2008), pp. 1–26.
[27]P. Fouquet, B. Farago, K. H. Andersen, P. M. Bentley, G. Pastrello, I. Sutton, E. Thaveron, F. Thomas, E. Moskvin, and C. Pappas, "Design and experimental tests of a novel neutron spin analyzer for wide angle spin echo spectrometers," Rev. Sci. Instrum. **80**(9), 095105 (2009).
[28]C. C. Finlay, S. Maus, C. D. Beggan, T. N. Bondar, A. Chambodut, T. A. Chernova, A. Chulliat, V. P. Golovkov, B. Hamilton, M. Hamoudi *et al.*, "International geomagnetic reference field: The eleventh generation," Geophys. J. Int. **183**(3), 1216–1230 (2010).
[29]T. Bigault, G. Delphin, A. Vittoz, V. Gaignon, and P. Courtois, "Recent polarizing supermirror projects at the ILL," J. Phys.: Conf. Ser. **528**, 012017 (2014).
[30]P. Böni, C. Schanzer, and M. Schneider, "Wide-angle transmission analyzer for polarized neutrons using equiangular spirals," Nucl. Instrum. Methods Phys. Res. Sect. A **966**, 163858 (2020).
[31]J. Y. Y. Lin, H. L. Smith, G. E. Granroth, D. L. Abernathy, M. D. Lumsden, B. Winn, A. A. Aczel, M. Aivazis, and B. Fultz, "MCViNE – An object oriented Monte Carlo neutron ray tracing simulation package," Nucl. Instrum. Methods Phys. Res. Sect. A **810**(C), 86–99 (2016).
[32]J. Y. Y. Lin, F. Islam, G. Sala, I. Lumsden, H. Smith, M. Doucet, M. B. Stone, D. L. Abernathy, G. Ehlers, J. F. Ankner *et al.*, "Recent developments of MCViNE and its applications at SNS," J. Phys. Commun. **3**(8), 085005 (2019).
[33]I. A. Zaliznyak, A. T. Savici, V. Ovidiu Garlea, B. Winn, U. Filges, J. Schneeloch, J. M. Tranquada, G. Gu, A. Wang, and C. Petrovic, "Polarized neutron scattering on HYSPEC: The HYbrid SPECtrometer at SNS," J. Phys.: Conf. Ser. **862**(1), 012030 (2017).
[34]A. Arbe, G. J. Nilsen, J. R. Stewart, F. Alvarez, V. G. Sakai, and J. Colmenero, "Coherent structural relaxation of water from meso- to intermolecular scales measured using neutron spectroscopy with polarization analysis," Phys. Rev. Res. **2**(2), 022015 (2020).